

ParaExp using Leapfrog as Integrator for High-Frequency Electromagnetic Simulations

M. Merkel*, I. Niyonzima*,[†], and S. Schöps*,[†]

*Graduate School of Computational Engineering (GSC CE), Technische Universität Darmstadt, Germany.

[†]Institut für Theorie Elektromagnetischer Felder (TEMF), Technische Universität Darmstadt, Germany.

Abstract—Recently, ParaExp was proposed for the time integration of linear hyperbolic problems. It splits the time interval of interest into sub-intervals and computes the solution on each sub-interval in parallel. The overall solution is decomposed into a particular solution defined on each sub-interval with zero initial conditions and a homogeneous solution propagated by the matrix exponential applied to the initial conditions. The efficiency of the method depends on fast approximations of this matrix exponential based on recent results from numerical linear algebra. This paper deals with the application of ParaExp in combination with Leapfrog to electromagnetic wave problems in time-domain. Numerical tests are carried out for a simple toy problem and a realistic spiral inductor model discretized by the Finite Integration Technique.

Index Terms—ParaExp, Leapfrog, Parallel-in-time method, Electromagnetic waves

I. INTRODUCTION

The simulation of high-frequency electromagnetic problems is often carried out in frequency domain. This choice is motivated by the linearity of the underlying governing equations. However, the solution of problems in frequency domain may require the resolution of very large linear systems of equations and this becomes particularly inconvenient for broadband simulations such that approximations like model order reduction are typically used, e.g. [20, 10, 19]. The coupling with nonlinear time-dependent systems and the computation of transients are other cases where time-domain simulations outperform frequency-domain simulations.

On the other hand, the numerical complexity resulting from time-domain simulations may also become prohibitively expensive. Parallelization in ‘space’, e.g., matrix-vector multiplications corresponding to the application of the curl operator, using multicore architectures is well established in academic and industrial software environments [7]. However, the parallelization efficiency eventually saturates with increasing number of cores depending on the memory bandwidth of the involved hardware. Time-domain parallelization is a promising extension to domain decomposition in space.

The development and application of parallel-in-time methods dates back more than 50 years, see [18]. These methods can be direct [6, 11] or iterative [14, 16]. They can also be well suited for small scale parallelization [17, 24] or large parallelization [11, 16]. Recently, the *Parareal method*

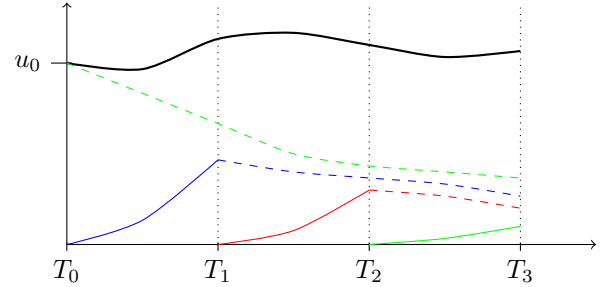


Fig. 1. Schematic view of the decomposition of time and solution. Vertical dotted lines denote the sub-intervals, solid lines represent the solution of the inhomogeneous sub-problems and dashed lines represent the solution of the homogeneous sub-problems. The thick black line represents the overall solution. Colors indicate the employed processors, cf. [11]

gained interest [14, 12]. In its initial version, Parareal was developed for large scale semi-discretized parabolic partial differential equations (PDEs). It involves the splitting of the time interval and the resolution of the governing ordinary differential equation (ODE) in parallel on each sub-interval using a fine propagator which can be any classical time-stepper with a fine time grid. A coarse propagator distributes the initial conditions for each sub-interval during the Parareal iterations. It is typically obtained by a time stepper with a coarse grid on the entire time interval. Parareal iterates the resolution of both the coarse and the fine problems until convergence.

Most parallel-in-time methods fail for hyperbolic problems. In the case of Parareal, analysis has shown that it may lead to the *beating* phenomenon depending on the structure of the system matrix [9]. It may even become unstable if the eigenvalues of the matrix are purely imaginary which is the case in the presence of undamped electromagnetic waves.

In this paper we apply the *ParaExp method* from [11] for the parallelization of time-domain resolutions of hyperbolic equations that govern the electromagnetic wave problems as initially proposed in [15].

The method splits the time interval into sub-intervals and solves smaller problems on each sub-interval as visualized in Figure 1. Using the theory of linear ordinary differential equations, the total solution for each sub-interval is decomposed into particular solution with zero initial conditions and homogeneous solutions with initial conditions from previous intervals.

The paper is organized as follows: in Section II we introduce Maxwell’s equations and derive the governing system of ODEs for the wave equation obtained by the Finite Integration

Corresponding author: Melina Merkel, Technische Universität Darmstadt Institut für Theorie Elektromagnetischer Felder, Schloßgartenstr. 8 64289 Darmstadt (anna_melina.merkel@stud.tu-darmstadt.de)

Technique (FIT). This system is then used in Section III for the presentation of the ParaExp method following the lines of [11]. The mathematical framework is briefly sketched and the details of the algorithm are discussed. The combination of ParaExp with Leapfrog is proposed. Section IV deals with numerical examples. We consider two applications: a simple wave guide problem and a realistic spiral inductor model discretized by the Finite Integration Technique. The examples are investigated in terms of efficiency, energy conservation and frequency spectrum.

II. SPACE AND TIME DISCRETIZATION OF MAXWELL'S EQUATIONS

In an open, bounded domain $\Omega \subset \mathbb{R}^3$ and $t \in \mathcal{J} = (t_0, t_{\text{end}}] \subset \mathbb{R}_{\geq 0}$, the evolution of electromagnetic fields is governed by Maxwell's equations on $\Omega \times \mathcal{J}$, see e.g. [13]:

$$\begin{aligned} \nabla \times \mathbf{E} &= -\partial_t \mathbf{B}, & \nabla \times \mathbf{H} &= \partial_t \mathbf{D} + \mathbf{J}, \\ \nabla \cdot \mathbf{B} &= 0, & \nabla \cdot \mathbf{D} &= \rho \end{aligned} \quad (1)$$

$$\nabla \cdot \mathbf{B} = 0, \quad \nabla \cdot \mathbf{D} = \rho \quad (2)$$

with suitable initial and boundary conditions at time t_0 and $\partial\Omega$, respectively. In presence of linear materials, these equations are completed by constitutive laws [13]:

$$\mathbf{D} = \varepsilon \mathbf{E}, \quad \mathbf{J} = \sigma \mathbf{E} + \mathbf{J}_s, \quad \mathbf{B} = \mu \mathbf{H}. \quad (3)$$

In these equations, \mathbf{H} is the magnetic field [A/m], \mathbf{B} the magnetic flux density [T], \mathbf{E} the electric field [V/m], \mathbf{D} the electric flux density [C/m²], \mathbf{J} , $\mathbf{J}_\sigma = \sigma \mathbf{E}$, $\mathbf{J}_d = \partial_t \mathbf{D}$ and \mathbf{J}_s are the total, Ohmic, displacement and electric source current densities [A/m²], ρ is the electric charge density [C/m³]. The material properties σ , ε and μ are the electric conductivity, the electric permittivity and the magnetic permeability, respectively. In this paper, we consider electromagnetic wave propagation in non-conducting media which are free of charges, i.e., $\sigma \equiv 0$ and $\rho \equiv 0$.

The space discretization of Maxwell's equations (2)-(3) using the Finite Integration Technique (FIT) [22, 23] on a staggered grid pair with primal $n = n_x \cdot n_y \cdot n_z$ grid points leads to the equations

$$\mathbf{C} \widehat{\mathbf{e}} = -d_t \widehat{\mathbf{b}}, \quad \widetilde{\mathbf{C}} \widehat{\mathbf{h}} = d_t \widehat{\mathbf{d}} + \widehat{\mathbf{j}}, \quad (4)$$

$$\widetilde{\mathbf{S}} \widehat{\mathbf{b}} = \mathbf{0}, \quad \mathbf{S} \widehat{\mathbf{d}} = \mathbf{q} \quad (5)$$

where $\mathbf{C}, \widetilde{\mathbf{C}} \in \mathbb{R}^{n_{\text{dof}} \times n_{\text{dof}}}$ are the discrete curl operators, $\mathbf{S}, \widetilde{\mathbf{S}} \in \mathbb{R}^{n \times n_{\text{dof}}}$ the discrete divergence operators, which are all defined on the primal and dual grid, respectively ($n_{\text{dof}} \approx 3n$). The fields are semi-discretely given by $\widehat{\mathbf{e}}, \widehat{\mathbf{h}}, \widehat{\mathbf{d}}, \widehat{\mathbf{j}}, \widehat{\mathbf{b}} : \mathcal{J} \rightarrow \mathbb{R}^{n_{\text{dof}}}$ and $\mathbf{q} : \mathcal{J} \rightarrow \mathbb{R}^n$ corresponding to electric and magnetic voltages, electric fluxes, electric currents, magnetic fluxes and electric charges, respectively. They are linked by the material relations

$$\widehat{\mathbf{d}} = \mathbf{M}_\varepsilon \widehat{\mathbf{e}}, \quad \widehat{\mathbf{j}} = \mathbf{M}_\sigma \widehat{\mathbf{e}} + \widehat{\mathbf{j}}_s, \quad \widehat{\mathbf{b}} = \mathbf{M}_\mu \widehat{\mathbf{h}} \quad (6)$$

where \mathbf{M}_ε and \mathbf{M}_μ are diagonal positive-definite material matrices of permittivities ε and permeabilities μ . The conductivity matrix \mathbf{M}_σ will not be considered as mentioned above.

The system (4-6) can be rewritten as an initial value problem (IVP)

$$\mathbf{M} d_t \bar{\mathbf{u}} + \mathbf{K} \bar{\mathbf{u}} = \bar{\mathbf{g}}(t), \quad \bar{\mathbf{u}}(t_0) = \bar{\mathbf{u}}_0. \quad (7)$$

with unknown voltages $\bar{\mathbf{u}}^\top := [\widehat{\mathbf{h}}^\top, \widehat{\mathbf{e}}^\top]$, given excitation $\bar{\mathbf{g}}^\top := [\mathbf{0}, \widehat{\mathbf{j}}_s^\top]$ and the matrices

$$\mathbf{M} := \begin{bmatrix} \mathbf{M}_\mu & \mathbf{0} \\ \mathbf{0} & \mathbf{M}_\varepsilon \end{bmatrix}, \quad \mathbf{K} := \begin{bmatrix} \mathbf{0} & \mathbf{C} \\ -\widetilde{\mathbf{C}} & \mathbf{0} \end{bmatrix}. \quad (8)$$

Exploiting a similarity transformation by the matrix $\mathbf{T} := \text{blkdiag}(\mathbf{M}_\mu^{1/2}, \mathbf{M}_\varepsilon^{1/2})$ allows to rewrite (7) as

$$d_t \mathbf{u} = \mathbf{A} \mathbf{u} + \mathbf{g}(t), \quad \mathbf{u}(t_0) = \mathbf{u}_0 \quad (9)$$

in the new unknowns $\mathbf{u}^\top = [\mathbf{M}_\mu^{1/2} \widehat{\mathbf{h}}^\top, \mathbf{M}_\varepsilon^{1/2} \widehat{\mathbf{e}}^\top]$ with the skew-symmetric stiffness matrix

$$\mathbf{A} = \begin{bmatrix} \mathbf{0} & -\mathbf{M}_\mu^{-1/2} \mathbf{C} \mathbf{M}_\varepsilon^{-1/2} \\ \mathbf{M}_\varepsilon^{-1/2} \widetilde{\mathbf{C}} \mathbf{M}_\mu^{-1/2} & \mathbf{0} \end{bmatrix}. \quad (10)$$

and right-hand-side $\mathbf{g}^\top = [\mathbf{0}, \mathbf{M}_\varepsilon^{-1/2} \widehat{\mathbf{j}}_s^\top]$. One advantage of the transformed system (9) is that \mathbf{A} is normal, i.e., $\mathbf{A} \mathbf{A}^\top = \mathbf{A}^\top \mathbf{A}$ and one shows straightforwardly that all eigenvalues are imaginary.

A. Leapfrog

For high-frequency electromagnetic initial value problems one typically employs the Leapfrog scheme (or equivalently Störmer-Verlet) to solve the semi-discrete system (7). If the initial condition

$$\widehat{\mathbf{e}}^{(0)} = \widehat{\mathbf{e}}_0 \quad \text{and} \quad \widehat{\mathbf{h}}^{(\frac{1}{2})} = \widehat{\mathbf{h}}_{1/2}$$

is given, the Leapfrog update equations read time step $m \in \{0, \dots, n_t - 1\}$

$$\begin{aligned} \widehat{\mathbf{e}}^{(m+1)} &= \widehat{\mathbf{e}}^{(m)} + \Delta t \mathbf{M}_\varepsilon^{-1} \left(\widetilde{\mathbf{C}} \widehat{\mathbf{h}}^{(m+\frac{1}{2})} - \widehat{\mathbf{j}}^{(m+\frac{1}{2})} \right), \\ \widehat{\mathbf{h}}^{(m+\frac{3}{2})} &= \widehat{\mathbf{h}}^{(m+\frac{1}{2})} - \Delta t \mathbf{M}_\mu^{-1} \widetilde{\mathbf{C}} \widehat{\mathbf{e}}^{(m+1)} \end{aligned}$$

for the electric and magnetic voltages $\widehat{\mathbf{e}}^{(m)}, \widehat{\mathbf{h}}^{(m+\frac{1}{2})}$ at time points t_m and $t_{m+\frac{1}{2}}$ with step size Δt . The scheme is (up to scaling) equivalent to Yee's Finite-Difference-Time-Domain scheme [25]. Each equation applies the discretized curl operator and a few vector additions and scalar multiplications of complexity $\mathcal{O}(n_{\text{dof}})$. In the following discussion the focus will lie on the sparse-matrix-vector-multiplications (SMVP) as they are typically the most heavy operation, i.e., the cost of Leapfrog in terms of SMVP is given as

$$C_{\text{LF}} = 2 \cdot n_t \quad (11)$$

while additions and scalar multiplications are disregarded.

Leapfrog's time-stepping scheme is only conditionally stable and the maximal stable time step size Δt is limited by the Courant-Friedrichs-Lewy (CFL) condition. A sharp bound is given by the largest absolute eigenvalue of \mathbf{A} , i.e.,

$\lambda_{\max} = \|\mathbf{A}\|_2$ since \mathbf{A} is normal. In practice, one estimates the value by

$$\Delta t \leq \Delta t_{\text{CFL}} = \min_j \left(\sqrt{\frac{\varepsilon_j \mu_j}{\frac{1}{\Delta x_j^2} + \frac{1}{\Delta y_j^2} + \frac{1}{\Delta z_j^2}}} \right), \quad (12)$$

where j is the index of the grid cells and Δx_j Δy_j and Δz_j their spatial dimensions.

One remarkable property of the Leapfrog scheme is energy preservation (or symplecticity). Let us define the discrete magnetic and electric energies as follows

$$\begin{aligned} \langle \widehat{\mathbf{h}}^{(m)}, \widehat{\mathbf{h}}^{(n)} \rangle_{\mu} &:= (\widehat{\mathbf{h}}^{(m)})^{\top} \mathbf{M}_{\mu} \widehat{\mathbf{h}}^{(n)} \\ \langle \widehat{\mathbf{e}}^{(m)}, \widehat{\mathbf{e}}^{(n)} \rangle_{\varepsilon} &:= (\widehat{\mathbf{e}}^{(m)})^{\top} \mathbf{M}_{\varepsilon} \widehat{\mathbf{e}}^{(n)}. \end{aligned} \quad (13)$$

Using those energies and disregarding source currents, i.e. $\widehat{\mathbf{j}}_s \equiv 0$, one can show

$$\begin{aligned} \langle \widehat{\mathbf{e}}^{(m+1)}, \widehat{\mathbf{e}}^{(m+\frac{3}{2})} \rangle_{\varepsilon} + \langle \widehat{\mathbf{h}}^{(m+1)}, \widehat{\mathbf{h}}^{(m+\frac{3}{2})} \rangle_{\mu} \\ = \langle \widehat{\mathbf{e}}^{(m)}, \widehat{\mathbf{e}}^{(m+\frac{1}{2})} \rangle_{\varepsilon} + \langle \widehat{\mathbf{h}}^{(m)}, \widehat{\mathbf{h}}^{(m+\frac{1}{2})} \rangle_{\mu} \end{aligned} \quad (14)$$

where the electric and magnetic voltages must be consistently interpolated as $\widehat{\mathbf{e}}^{(m+\frac{1}{2})} := (\widehat{\mathbf{e}}^{(m)} + \widehat{\mathbf{e}}^{(m+1)})/2$ and $\widehat{\mathbf{h}}^{(m)} := (\widehat{\mathbf{h}}^{(m-\frac{1}{2})} + \widehat{\mathbf{h}}^{(m+\frac{1}{2})})/2$, see e.g. [4].

III. THE PARAREXP ALGORITHM

In this section we develop based on [11] the ideas of the ParaExp method for the system of ODEs in the form (9)

$$d_t \mathbf{u} = \mathbf{A} \mathbf{u} + \mathbf{g}(t) \quad \mathbf{u}(t_0) = \mathbf{u}_0.$$

Applying the method of variation of constants leads to the solution

$$\mathbf{u}(t) = \exp(t\mathbf{A})\mathbf{u}_0 + \int_0^t \exp((t-\tau)\mathbf{A})\mathbf{g}(\tau)d\tau \quad (15)$$

where $\exp(t\mathbf{A})\mathbf{u}_0$ is the homogeneous solution due to initial conditions and the convolution product is the particular solution resulting from the presence of the source term $\mathbf{g}(t)$. The last term of (15) is more difficult to compute than the first one. However, thanks to the linearity of the problem and the superposition principle, $\mathbf{u}(t)$ can be written as $\mathbf{u}(t) = \mathbf{v}(t) + \mathbf{w}(t)$ where the particular solution $\mathbf{v}(t)$ is governed by

$$d_t \mathbf{v} = \mathbf{A} \mathbf{v} + \mathbf{g}(t) \quad \mathbf{v}(t_0) = \mathbf{0} \quad (16)$$

and the homogeneous solution $\mathbf{w}(t)$ is governed by

$$d_t \mathbf{w} = \mathbf{A} \mathbf{w} + \mathbf{0} \quad \mathbf{w}(t_0) = \mathbf{u}_0. \quad (17)$$

The ParaExp method takes advantage of this decomposition. The time interval $\mathcal{J} = (0, T]$ is partitioned into sub-intervals $\mathcal{J}_j = (T_{j-1}, T_j]$ with $j = 1, 2, \dots, p$, $t_0 = T_0 < T_1 < T_2 < \dots < T_p = t_{\text{end}}$ and p the number of CPUs. The following solutions are then computed on each CPU: a particular solution $\mathbf{v}_j : \mathcal{J}_j \rightarrow \mathbb{R}^{n_{\text{dof}}}$ governed by

$$d_t \mathbf{v}_j = \mathbf{A} \mathbf{v}_j + \mathbf{g}(t) \quad \mathbf{v}_j(T_{j-1}) = \mathbf{0} \quad (18)$$

and a homogeneous solution $\mathbf{w}_j : \mathcal{J}_j \rightarrow \mathbb{R}^{n_{\text{dof}}}$ governed by

$$d_t \mathbf{w}_j = \mathbf{A} \mathbf{w}_j + \mathbf{0} \quad \mathbf{w}_j(T_{j-1}) = \mathbf{v}_{j-1}(T_{j-1}). \quad (19)$$

Input: system matrix \mathbf{A} , source term $\mathbf{g}(t)$, initial value \mathbf{u}_0 , time interval \mathcal{J} , number of processors p

Output: solution $\mathbf{u}(t)$

```

1 begin
2   partition  $\mathcal{J}$  into intervals  $\mathcal{J}_j$ ,  $j = 0, \dots, p$ ,
3   # begin the parallel loop (index  $j$ )
4   parfor ( $j \leftarrow 1$  to  $p$ ) do
5      $\mathbf{v}_j \leftarrow$  solve
6      $\mathbf{v}'_j(t) = \mathbf{A} \mathbf{v}_j(t) + \mathbf{g}(t)$ ,  $\mathbf{v}_j(T_{j-1}) = 0$ ,  $t \in \mathcal{J}_j$ 
7     using a time stepper
8     if  $j \neq p$  then
9        $\mathbf{w}_{j+1} \leftarrow \exp(\mathbf{A}(t - T_j)) \mathbf{v}_j(T_j)$  for all
10       $t \in (T_j, T_p]$ 
11    else
12       $\mathbf{w}_1 \leftarrow \exp(\mathbf{A}(t - T_0)) \mathbf{u}_0$  for all  $t \in (T_0, T_p]$ 
13    end
14  end
15 end

```

Fig. 2. Pseudocode for the ParaExp Algorithm

Problems (18) can be solved in parallel by any time stepping method as only trivial initial conditions must be provided. In this paper Leapfrog is employed as discussed in Section II-A. The solutions for (19) can be given analytically by

$$\mathbf{w}_j(t) = \exp(t\mathbf{A})\mathbf{v}_{j-1}(T_{j-1}) \quad (20)$$

where the initial condition is the final solution $\mathbf{v}_{j-1}(T_{j-1})$ of the previous interval. It is therefore highly recommended to compute $\mathbf{v}_{j-1}(t)$ and $\mathbf{w}_j(t)$ on the same CPU to avoid communicational costs. Using the superposition principle, the total solution can be expanded as:

$$\mathbf{u}(t) = \mathbf{v}_j(t) + \sum_{i=1}^j \mathbf{w}_i(t) \quad \text{with } j \text{ s.t. } t \in \mathcal{J}_j. \quad (21)$$

Figure 1 shows the time decomposition of IVP into particular solutions (solid lines) and homogeneous solutions (dashed lines) for a case with 3 CPUs. The two steps of the ParaExp method are described in the Algorithm shown in Figure 2.

A. Approximation of the matrix exponential

A critical point of the method is the efficient computation of equation (20) by the matrix exponential. A straight forward evaluation of the exponential followed by the multiplication with the vector of initial conditions is computationally very costly, especially for large matrices such as the matrices obtained by spatial discretization of the wave problem. Instead, efficient approximations of the action of the matrix exponential on initial condition vectors are used. Examples of such methods are the Krylov subspace based methods as used in [11], Higham's function [1] and Leja's method [5].

The Krylov subspace based methods (see [11]) require the evaluation of Krylov subspaces $\mathcal{K}^l(\mathbf{S}, \mathbf{b}) := \{\mathbf{b}, \mathbf{S}\mathbf{b}, \dots, \mathbf{S}^{l-1}\mathbf{b}\}$. These subspaces involve the evaluation of the matrix

$$\mathbf{S} := (\mathbf{I} - \mathbf{A}/\sigma)^{-1} \mathbf{A} \in \mathbb{C}^{2n_{\text{dof}} \times 2n_{\text{dof}}} \quad (22)$$

with $\sigma \in \mathbb{C}$ and its multiplication with the vector \mathbf{b} which is for example given by some solution $\mathbf{v}_j(t)$. If $\sigma \neq \infty$, one may approximate the action of the exponential with a rather small n but the computational costs of solving the large linear systems in (22) become prohibitive. The choice $\sigma = \infty$ leads to $\mathcal{K}^n(\mathbf{S}, \mathbf{b}) = \mathcal{K}^n(\mathbf{A}, \mathbf{b})$ and avoids matrix inversions but typically requires a rather large Krylov subspace in practice. In either case, the computational cost associated with the Krylov subspace based methods have been rather large such that we focus on Higham's and Leja's method in the following.

Both methods use two main ingredients. The first ingredient is the *scaling* of the matrix exponential:

$$\begin{aligned} \exp(t\mathbf{A})\mathbf{b} &= (\exp(t\mathbf{A}/s))^s \mathbf{b} \\ &\approx (P(t\mathbf{A}/s))^s \mathbf{b} =: \exp(t(\mathbf{A} + \Delta\mathbf{A}))\mathbf{b} \end{aligned}$$

which reduces the spectrum of the scaled matrix $\exp(t\mathbf{A}/s)$ around the origin thus allowing its efficient approximation by polynomial interpolations P such as Taylor's expansion. The second ingredient is the use of a *recurrence equation* that involves SMVPs. In the case Higham's function, the recurrence equation reads:

$$\mathbf{b}_{i+1} = T_m(t\mathbf{A}/s)\mathbf{b}_i, i = 0, \dots, s-1, \mathbf{b}_0 = \mathbf{b}.$$

where T_m is Taylor's truncated polynomial of order m , i.e.,

$$T_m(t\mathbf{A}/s) = \sum_{j=0}^m \frac{(t\mathbf{A}/s)^j}{j!}.$$

Leja's method uses interpolation which is a Newton-Cotes interpolation polynomial $L_{m,c}$ defined on the set of Leja's points [5]. Similarly to Chebyshev's approach, the points are chosen such that the condition number of the polynomial remains small when the polynomial order m is increasing. In the case of the wave equation with imaginary eigenvalues, the interpolation is defined on an interval in the complex plane. The resulting recurrence equation reads

$$\mathbf{b}_{i+1} = L_{m,c}(t\mathbf{A}/s)\mathbf{b}_i, i = 0, \dots, s-1, \mathbf{b}_0 = \mathbf{b}.$$

Leja's interpolation $L_{m,c}$ reduces to the Taylor series for $c = 0$ but it performs better than Higham's functions for normal matrices with a value of $c \neq 0$. In both cases, the approximate solution is derived as $\mathbf{u} = \mathbf{b}_s$. The parameters m, s (and c in the case of Leja's method) are chosen so as to minimize the computational cost given by the number of SMVPs

$$C_{\text{Leja}} = n_{\text{Leja}},$$

with the condition $\|\Delta\mathbf{A}\| \leq \varepsilon_A \|\mathbf{A}\|$ where ε_A is a prescribed tolerance. This cost is dominated by the approximation of the matrix exponential with $n_{\text{Leja}} \approx sm$. The approximation involves s multiplications of the Taylor polynomial $P(t\mathbf{A}/s)$ of order m . An additional cost results from the evaluation of

the optimal parameters m, s and c involving the computation of the norm of the matrix \mathbf{A} (see [1]). Both algorithms also use additional preprocessing steps (shifting and balancing of the matrix) and an early termination of the iteration in the polynomial interpolations.

B. Reconstruction of voltages on staggered grids

When solving (18) with Leapfrog, electric and magnetic voltages are allocated on staggered time grids and it has been shown in Section II-A that this is crucial for energy conservation. Therefore we propose to modify the reconstruction (21) in the case of Leapfrog in the obvious manner for the total electric grid voltages as

$$\mathbf{e}^{(m+1)} = \mathbf{e}_j^{(m+1)} + [\mathbf{0}, \mathbf{M}_\varepsilon^{-1/2}] \sum_{i=1}^j \mathbf{w}_i(t^{m+1}) \quad (23)$$

for $t^{m+1} \in J_j$ and the total magnetic grid voltages

$$\mathbf{h}^{(m+\frac{1}{2})} = \mathbf{h}_j^{(m+\frac{1}{2})} + [\mathbf{M}_\mu^{-1/2}, \mathbf{0}] \sum_{i=1}^j \mathbf{w}_i(t^{m+\frac{1}{2}}) \quad (24)$$

for $t^{m+\frac{1}{2}} \in J_j$ where $\mathbf{e}_j^{(m+1)}$ and $\mathbf{h}_j^{(m+\frac{1}{2})}$ are the solutions of (18) at time t^{m+1} and $t^{m+\frac{1}{2}}$ using Leapfrog and the matrices $[\mathbf{0}, \mathbf{M}_\varepsilon^{-1/2}]$ and $[\mathbf{M}_\mu^{-1/2}, \mathbf{0}]$ are used to extract and transform the respective components from the solution \mathbf{w} of (19). Leapfrog is initialized with $\mathbf{e}_0 = \mathbf{0}$ and $\mathbf{h}_{\frac{1}{2}} = \mathbf{0}$ for all time intervals J_j .

C. Discussion of the numerical costs

The computational costs of Paraexp can be split into three categories: (i) execution of Leapfrog, (ii) propagation of initial values by the matrix exponential and (iii) two transformations (9) for initial and end values at each interval. The effective number of SMVPs, i.e., disregarding operations carried out in parallel, is given by

$$C_{\text{proc}} = \frac{2}{p} n_t + n_{\text{Leja}} + 2, \quad (25)$$

if the same number of time steps is performed on each processor. When increasing the number of processors p , the costs of Leapfrog can be disregarded and the only remaining costs are SMVPs due to Leja for the longest time interval, i.e., for propagating the initial value from t_0 to t_{end} .

D. Error analysis

Neglecting the round-off errors, the contribution to the main error of ParaExp method from the j^{th} CPU has two main contributions.

The first contribution is the truncation error resulting from the Leapfrog scheme used for solving the non-homogeneous problem on the sub-interval $J_j = (T_{j-1}, T_j]$. There is no error in the initial value since we start from the trivial initial condition. The resulting numerical solution $\hat{\mathbf{v}}_j$ is given by

$$\hat{\mathbf{v}}_j = \mathbf{v}_j + \Delta\mathbf{v}_j, \quad (26)$$

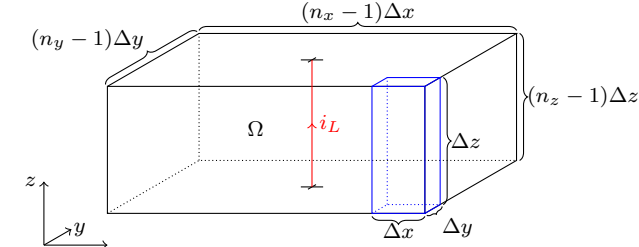


Fig. 3. Domain Ω of the wave problem with a hexahedral mesh

where \mathbf{v}_j is the exact solution of the problem and $\Delta \mathbf{v}_j \sim \mathcal{O}(\Delta t)^2$ is the truncation error. This solution is then used as an initial condition for the homogeneous problem.

The second contribution is the approximation error of the matrix exponential on the interval $(T_j, T]$. It can be analyzed using the backward error analysis as introduced by Higham, see Section III-A:

$$\hat{\mathbf{w}}_j = \mathbf{w}_j + \Delta \mathbf{w}_j = \exp(t(\mathbf{A} + \Delta \mathbf{A})) \hat{\mathbf{v}}_j(T_j) \quad (27)$$

with $\hat{\mathbf{w}}_j$ the numerical solution obtained by approximating the exponential of the matrix, \mathbf{w}_j the exact homogeneous solution and $\Delta \mathbf{w}_j$ the approximation error. The contribution of the j^{th} CPU to the total numerical solution is therefore given by

$$\begin{aligned} \hat{\mathbf{u}}_j &= \mathbf{u}_j + \Delta \mathbf{u}_j = \exp(t\mathbf{A}) \mathbf{v}_j + \Delta \mathbf{u}_j \\ &= \exp(t(\mathbf{A} + \Delta \mathbf{A})) (\mathbf{v}_j + \Delta \mathbf{v}_j), \end{aligned}$$

where $\mathbf{u}_j = \mathbf{v}_j + \mathbf{w}_j$ is the exact solution. The analysis developed in Section 4 of [1] can be used to quantify these errors and to adjust the relative tolerance of Leja's method so that both errors are of the same magnitude. Applying Lemma 4.2 from [1] together with formula (4.5) to the action of the matrix exponential with $\|\Delta \mathbf{A}\| \leq \varepsilon_A \|\mathbf{A}\|$ where ε_A is a prescribed relative tolerance and assuming that $\|\Delta \mathbf{v}_j\| \leq \varepsilon_B \|\mathbf{w}_j\|$ with $\varepsilon_B = \beta \Delta t^2$, the following result can be derived:

$$\frac{\|\Delta \mathbf{u}_j\|_2}{\|\mathbf{u}_j\|_2} \leq \frac{\|e^{t\mathbf{A}}\|_F \|\mathbf{v}_j\|_2}{\|\mathbf{u}_j\|_2} \left(\frac{\varepsilon_B}{\varepsilon_A} + \kappa_{\text{exp}}(\mathbf{A}) \right)$$

where $\kappa_{\text{exp}}(\mathbf{A})$ is the condition number of the matrix exponential, i.e., $\kappa_{\text{exp}}(\mathbf{A}) = \|\mathbf{A}\|_2$ for normal matrices. For a fixed ε_B , both terms in the brackets become equal if

$$\frac{\varepsilon_B}{\varepsilon_A^*} = \kappa_{\text{exp}}(\mathbf{A}) = \|\mathbf{A}\|_2 \quad (28)$$

leading to the optimal value of the tolerance for the matrix exponential given by

$$\varepsilon_A^* = \frac{\beta \Delta t^2}{\kappa_{\text{exp}}(\mathbf{A})} = \frac{\beta \Delta t^2}{\|\mathbf{A}\|_2}. \quad (29)$$

IV. NUMERICAL TESTS

We consider two numerical tests for the validation: a two-dimensional cylindrical wave excited by a line current and a spiral inductor discretized by CST MICROWAVE STUDIO[®] based on the design proposed in [2, 7].

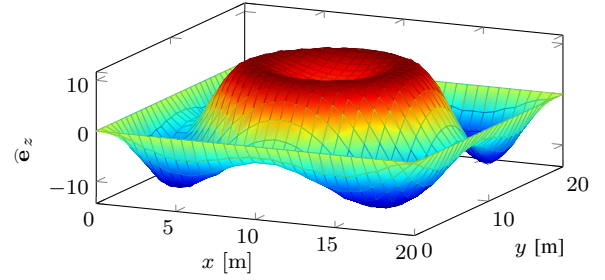


Fig. 4. The $\bar{\mathbf{e}}_z$ component of the wave at $t = 4.8 \cdot 10^{-8}$ s

A. Cylindrical two-dimensional wave

The two-dimensional cylindrical wave problem is depicted in Figure 3. The excitation is a line current in z -direction in the center of the domain Ω . The discretization is obtained by FIT as explained in Section II. A PEC boundary is assumed on the whole boundary $\partial\Omega$. The dimensions of the domain Ω are $L_x = L_y = 20$ m and $L_z = 1$ m. For the discretization we use $n_x = n_y = 41$, $n_z = 2$ for Leapfrog and Leja's method and $n_x = n_y = 121$, $n_z = 2$ for the reference numerical solution. This corresponds to $n_{\text{dof}} = 20\,172$ and $n_{\text{dof}} = 175\,692$ degrees of freedom, respectively.

The domain is filled with vacuum. The line current is a Gaussian function given by

$$i_L(t) = i_{\text{max}} \exp\left(-4 \left(\frac{t - \sigma_t}{\sigma_t}\right)^2\right) \quad (30)$$

with $i_{\text{max}} = 1$ A and $\sigma_t = 2 \cdot 10^{-8}$ s.

The differential equation of this problem is given by (7) and (8) with $\bar{\mathbf{g}}(t) = -[\mathbf{0}, \hat{\mathbf{j}}]^\top$, with $\hat{\mathbf{j}}$ being the discretized line current (30). We consider the a transformed ODE (9) with \mathbf{A} being normal. The $\bar{\mathbf{e}}_z$ component of the calculated wave can be seen in Figure 4 at time $t = 4.4 \cdot 10^{-8}$ s.

Numerical experiments show that Leja's method outperforms Higham's approach and the Krylov subspace methods by a factor of 2 and 10, respectively. This is in agreement with the literature where Leja has been observed to perform best for normal matrices [5]. Therefore, we will only present results of Leja's method from now on.

Leapfrog and ParaExp cause two different kinds of error: the truncation error for Leapfrog is related to the time step whereas the error of ParaExp can be quantified using the backward error analysis as discussed above. Therefore it is crucial to choose the parameters of Leja's algorithm to make the comparison between Leapfrog and ParaExp as fair as possible.

For a given spatial mesh, the time step for Leapfrog is chosen according to the CFL criterion (12). The tolerance ε_A of Leja's algorithm has been increased such that the error $\Delta \mathbf{v}$ due to Leapfrog still dominates over the error due to the matrix exponential $\Delta \mathbf{w}$. Results are shown in Figure 5. In this figure, the costs of the Leapfrog scheme and Leja are compared on $\mathcal{J} = (0, T]$ with $T = 2 \cdot 10^{-7}$ s motivated by the reasoning given in (25): if $p \gg 1$ we neglect the cost of the Leapfrog scheme used for solving the non-homogeneous problem (18) and only consider the cost of the propagation of the matrix exponential on \mathcal{J} . As expected, the number of

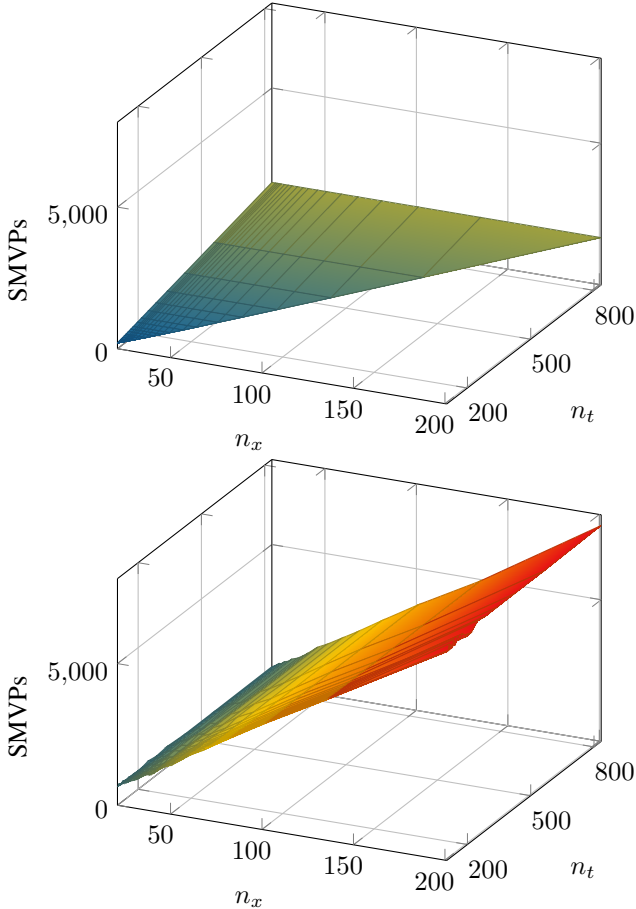


Fig. 5. Computational cost of Leapfrog and Leja's method for a uniform mesh. Top: cost for Leapfrog. Bottom: cost for Leja's method. The tolerance of Leja has been chosen as $1 \cdot 10^{-2}$

SMVPs of the Leapfrog algorithm is linearly proportional to the number of time steps n_t , see (11). The increase of the number of time steps n_t does not correspond to an increase of cost for Leja method as the matrix of the system and the time interval remain unchanged. A slight increase may however result from the evaluation of intermediate interpolations.

The increase of n_x which corresponds to the refinement of the spatial grid does not change the number of SMVPs for Leapfrog if Δt remains below Δt_{CFL} . Otherwise it increases linearly which is in good agreement with the estimate (12). For Leja's method, an even stronger linear increase of the number of SMVPs is observed also corresponding to the increase of the largest eigenvalue (28). In both cases the cost of each SMVP also increases due to the growing dimension n_{dof} of the sparse matrices.

The Leapfrog scheme is known to be very competitive when using homogeneous grids, however small elements may quickly deteriorate the efficiency. Therefore a second numerical experiment investigates the efficiency in the cases of increasing inhomogeneity. The mesh of Figure 3 was kept except for one element whose dimensions have been modified so that the ratio k between the size of the biggest element over the size of the smallest element of the mesh lies in the

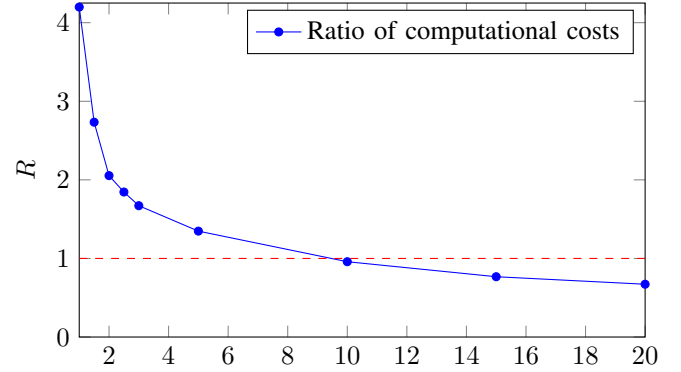


Fig. 6. Ratio between computational costs of Leapfrog and Leja's method for a non-uniform mesh and comparable accuracies as defined in (31).

interval $[1, 20]$. The ratio of the computational cost

$$R(k) = \frac{C_{\text{Leja}}(k)}{C_{\text{LF}}(k)} \quad (31)$$

is given as the quotient of the number of SMVPs for performing Leja and Leapfrog on the whole time interval \mathcal{J} in dependency of the non-uniformity of the mesh. Figure 6 shows a better performance for ParaExp over Leapfrog for large values of k . This suggests a better performance of ParaExp for highly non-uniform grids, although also Leja is depending via κ_{exp} on the eigenvalues of the operator \mathbf{A} .

In a third experiment the energy conservation is numerically analyzed. ParaExp itself is as energy conserving as the methods used for time integration and propagation. While this is well understood for Leapfrog as discussed in Section II-A, it is not clear for the Leja method. Figure 8 shows the energy for Leapfrog computed according to (14) and for Paraexp using

$$E(t) := \langle \widehat{\mathbf{h}}(t), \widehat{\mathbf{h}}(t) \rangle_{\mu} + \langle \widehat{\mathbf{e}}(t), \widehat{\mathbf{e}}(t) \rangle_{\epsilon}$$

with the averaging from (23). It can be seen that the energy remains constant once the excitation is vanishing, i.e., for $t \in \mathcal{J}$ such that $i_L(t) = 0$. The electromagnetic energy present in the system remains constant and almost independent of the spatial refinement.

In order to analyze the accuracy of the ParaExp method the frequency spectrum of the electric field obtained by ParaExp and Leapfrog are compared in Figure 7. It can be observed that ParaExp adds high frequency noise to the solution. A side effect of those high frequencies is a potentially unphysical increase of energy in the domain as observed in Fig. 8. This can be avoided by reducing the time step size Δt of the used Leapfrog algorithm. In this case using $\Delta t = \frac{\Delta t_{\text{CFL}}}{5}$ leads to a solution without high frequency noise.

B. Spiral inductor

The second test case is a spiral inductor model created with coplanar lines located on a substrate layer with an air bridge. The model is based on the design proposed in [2] and the corresponding example from the CST tutorial on transient analysis which advocates the usage of 3D field simulation instead of circuit models, cf. [7]. The geometry of the problem is illustrated in Figure 9 with the dimensions: $7 \cdot 10^{-4} \text{ m} \times$

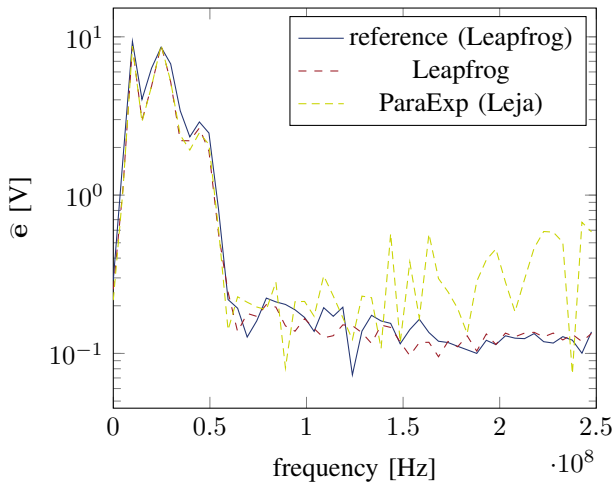


Fig. 7. Frequency spectrum of \hat{e} for Leapfrog and ParaExp (6 parallel threads, Leja).

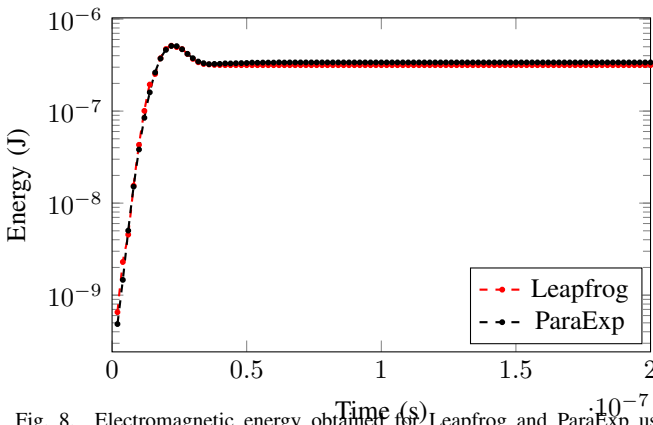


Fig. 8. Electromagnetic energy obtained for Leapfrog and ParaExp using Leja.

$4.75 \cdot 10^{-4} \text{ m} \times 2.5 \cdot 10^{-5} \text{ m}$. The structure is discretized using a mesh with 406 493 mesh cells. The largest cell has the dimensions $8.9 \cdot 10^{-6} \text{ m} \times 8.9 \cdot 10^{-6} \text{ m} \times 8.8 \cdot 10^{-6} \text{ m}$ and the smallest cell has the dimensions $2 \cdot 10^{-6} \text{ m} \times 2 \cdot 10^{-6} \text{ m} \times 1.5 \cdot 10^{-6} \text{ m}$. The conductor is modeled by PEC, the substrate is given by a relative permittivity of $\epsilon_r = 12$. The domain is discretized using $n_{\text{dof}} = 1, 283, 040$ degrees of freedom for \hat{e} and \hat{h} respectively and excited by a sine wave at 50 GHz. The propagation of the results from t_0 to t_{end} by Leapfrog requires 21 654 SMVPs while Leja needs 34 864 SMVPs for the same interval, cf. Figure V. In other words, classical time-stepping by Leapfrog is approximately 1.6 times faster than the evaluation of the matrix exponential for this example and ParaExp does not pay off. Motivated by the results of Figure 6, a carefully chosen example with small geometric details may change the situation in favor of ParaExp but for a general problem Leapfrog remains the appropriate choice.

V. CONCLUSIONS

In this paper, the ParaExp method was used for parallelization of time domain simulation of the electromagnetic wave problem and its performances were compared to the

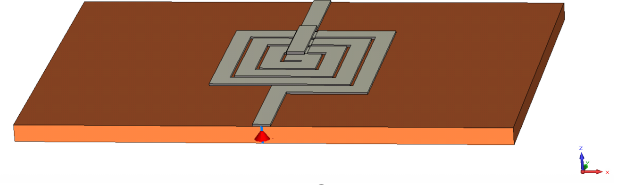


Fig. 9. CST MICROWAVE STUDIO[®] model of a spiral inductor based on [2]



Fig. 10. Number of SMVPs of Leja and Leapfrog to propagate the initial value from t_0 to t_{end}

performance of the Leapfrog scheme. The efficiency of ParaExp heavily depends on the approximation of the action of the matrix exponential to the vector of initial conditions and this approximation is the bottleneck of the method. Two methods were investigated for the approximation of the matrix exponential: Higham's function and Leja's method. In our applications, Leja's method was more efficient because the problem can be reformulated in terms of a normal system matrix. Numerical tests have shown that Leapfrog performs better than ParaExp with Leja for problems involving uniform meshes, but ParaExp can become more efficient than Leapfrog for problems involving highly non-uniform meshes. In contrast to Leapfrog the energy preservation of Paraexp does not only depend on the time stepper used but also on the approximation of the matrix exponential.

ACKNOWLEDGMENTS

The authors would like to thank Timo Euler, CST AG for the fruitful discussions on time domain simulations and Prof. Marco Caliani from the University of Verona for the discussion on the numerical implementation of Leja's method.

This work was supported by the German Funding Agency (DFG) by the grant 'Parallel and Explicit Methods for the Eddy Current Problem' (SCHO-1562/1-1), the 'Excellence Initiative' of the German Federal and State Governments and the Graduate School CE at Technische Universität Darmstadt.

REFERENCES

- [1] Al-Mohy, A. H., and N. J. Higham (2011), *Computing the action of the matrix exponential, with an application to exponential integrators*, SIAM Journal on Scientific Computing, 33(2), pp. 488–511.
- [2] Becks, T. and Wolff, I. (1992) *Analysis of 3-D metalization structures by a full-wave spectral-domain technique*, IEEE Transactions on Microwave Theory and Techniques: 40(12), pp. 2219–2227
- [3] Bossavit, A. (1998), *Computational Electromagnetism. Variational Formulations, Complementarity, Edge Elements*, Academic Press.

- [4] Bossavit, A. (1999), *Computational electromagnetism and geometry:(2): Network constitutive laws*, The Japan Society of Applied Electromagnetics and Mechanics, 7(3), pp. 294–301.
- [5] Caliari, Marco, et al. (2016) *The Leja method revisited: backward error analysis for the matrix exponential*, SIAM Journal on Scientific Computing 38(3): A1639–A1661.
- [6] Christlieb, A. J., C. B. Macdonald, and B. W. Ong (2010), *Parallel high-order integrators*, SIAM Journal on Scientific Computing, 32(2), pp. 818–835.
- [7] CST AG (2016), CST STUDIO SUITE 2016 <https://www.cst.com>
- [8] Eaton, J. W., et al. (2015), GNU Octave 4.0 Reference Manual.
- [9] Farhat, C., J. Cortial, C. Dastillung, and H. Bavestrello (2006), *Time-parallel implicit integrators for the near-real-time prediction of linear structural dynamic responses*, International Journal for Numerical Methods in Engineering, 67(5), pp. 697–724.
- [10] Floch, O., Sommer, A., Farle, O. and Dyczij-Edlinger, R. (2015) *Is model-order reduction viable for the broadband finite-element analysis of electrically large antenna arrays?*, Advances in Radio Science: ARS, 13, p.31.
- [11] Gander, M. J., and S. Güttel (2013), *ParaExp: A parallel integrator for linear initial-value problems*, SIAM Journal on Scientific Computing, 35(2), C123–C142.
- [12] Gander, M. J., and S. Vandewalle (2007), *Analysis of the Parareal time-parallel time-integration method*, SIAM Journal on Scientific Computing, 29(2), pp. 556–578.
- [13] Jackson, J. D. (1999), *Classical Electrodynamics*, Wiley.
- [14] Lions, J.-L., Y. Maday, and G. Turinici (2001), *A ‘Parareal’ in time discretization of PDEs*, Comptes Rendus de l’Academie des Sciences Series I Mathematics, 332(7), pp. 661–668.
- [15] Merkel, M., I. Niyonzima, and S. Schöps (2016), *An Application of ParaExp to Electromagnetic Waves*, Proceedings of 2016 URSI International Symposium on Electromagnetic Theory (EMTS), pp. 121–124.
- [16] Minion, M. (2011), *A hybrid Parareal spectral deferred corrections method*, Communications in Applied Mathematics and Computational Science, 5(2), pp. 265–301.
- [17] Miranker, W. L., and W. Liniger (1967), *Parallel methods for the numerical integration of ordinary differential equations*, Mathematics of Computation, 21(99), pp. 303–320.
- [18] Nievergelt, J. (1964), *Parallel methods for integrating ordinary differential equations*, Communications of the ACM, 7(12), pp. 731–733.
- [19] Paquay, Y., Geuzaine, C., Hasan, R. and Sabariego, R.V. (2016). *Reduced-Order Model Accounting for High-Frequency Effects in Power Electronic Components*. IEEE Transactions on Magnetics, 52(3), pp. 1–4.
- [20] Slone, R. D., Lee, R., and Lee, J.-F. (2003), *Broadband model order reduction of polynomial matrix equations using single-point well-conditioned asymptotic waveform evaluation: derivations and theory*, International Journal for Numerical Methods in Engineering, 58, pp. 2325–2342.
- [21] Treichl, T., and J. Corno (2017), *OdePkg, A Package for Solving Differential Equations with Octave*, <https://octave.sourceforge.io/odepkg/>.
- [22] Weiland, T. (1977), *A discretization model for the solution of Maxwell’s equations for six-component fields*, International Journal of Electronics and Communications, 31, pp. 116–120.
- [23] Weiland, T. (1996), *Time domain electromagnetic field computation with finite difference methods*, International Journal of Numerical Modelling: Electronic Networks, Devices and Fields, 9(4), pp. 295–319.
- [24] Womble, D. E. (1990), *A time-stepping algorithm for parallel computers*, SIAM Journal on Scientific and Statistical Computing, 11(5), pp. 824–837.
- [25] Yee, K. (1966), *Numerical solution of initial boundary value problems involving Maxwell’s equations in isotropic media* IEEE Transactions on antennas and propagation, 14(3), pp. 302–307.